



Article

Determination of the Geoid–Quasigeoid Separation Using GGI Method

Marek Trojanowicz ^{1,*} , Magdalena Owczarek-Wesołowska ¹ and Yan Ming Wang ²

¹ Institute of Geodesy and Geoinformatics, Wrocław University of Environmental and Life Sciences, C. K. Norwida 25, 50-375 Wrocław, Poland; magdalena.owczarek-wesolowska@upwr.edu.pl

² National Oceanic and Atmospheric Administration, National Geodetic Survey, 1315 East-West Highway, Silver Spring, MD 20910-3282, USA; yan.wang@noaa.gov

* Correspondence: marek.trojanowicz@upwr.edu.pl

Abstract: The determination of the geoid–quasigeoid separation (GQS) is most often based on the use of Bouguer gravity anomalies or disturbances with additional corrections, which allow for the determination of so-called complete or accurate GQS values. This study presents analyses related to an attempt to determine accurate GQS values using the GGI approach (based on the geophysical gravity inversion technique). This approach allows for the modeling of various parameters of the gravity field, and it also enables the determination of the GQS or geoid undulations. Such capabilities of the method have not yet been tested. In this study, the details of the GGI solution in terms of determining the GQS and the first results from tests performed in the area of the Colorado 1 cm geoid computation experiment are presented. The GQS values determined by the GGI approach were compared with the reference values determined previously using the complete classical approach. The differences between the compared values were small, with a standard deviation of 0.007 m, and the maximum differences reached 0.075 m. The analyses also revealed the significant impact of changes in the density of topographic masses on both the geoid undulations and GQS values determined using the GGI approach.

Keywords: geoid–quasigeoid separation; geoid model; gravity inversion approach; quasigeoid model



Citation: Trojanowicz, M.; Owczarek-Wesołowska, M.; Wang, Y.M. Determination of the Geoid–Quasigeoid Separation Using GGI Method. *Remote Sens.* **2024**, *16*, 816. <https://doi.org/10.3390/rs16050816>

Academic Editor: Amin Beiranvand Pour

Received: 23 January 2024

Revised: 21 February 2024

Accepted: 22 February 2024

Published: 26 February 2024



Copyright: © 2024 by the authors. Licensee MDPI, Basel, Switzerland. This article is an open access article distributed under the terms and conditions of the Creative Commons Attribution (CC BY) license (<https://creativecommons.org/licenses/by/4.0/>).

1. Introduction

The geoid–quasigeoid separation (GQS) is the difference between the normal height (H^N) and the orthometric height (H^o). It is necessary for the conversion of heights between the normal and orthometric height systems (Figure 1). It can be also necessary for the quasigeoid modeling process using geoid modeling methods, and vice versa. The exact formula for the GQS results from the difference between normal and orthometric heights and is defined by Equation (1) [1]:

$$N - \zeta = \frac{\bar{g} - \bar{\gamma}}{\bar{\gamma}} H^o, \quad (1)$$

where \bar{g} is the mean gravity between the geoid and the terrain surface along the plumb line within the topography, $\bar{\gamma}$ is the mean normal gravity between the ellipsoid and the telluroid, and N and ζ are the geoid undulation and the height anomaly, respectively.

The most important factor for the accuracy of GQS values determined according to Equation (1) is the accuracy of the determined \bar{g} value. Since the direct measurement of gravity along the plumb line is generally not possible, the \bar{g} value is determined with some approximation. This means that the GQS values are also determined inaccurately. A frequently used approximation of the GQS is related to Helmert's orthometric heights [1]:

$$N - \zeta \cong \frac{\Delta g_B}{\bar{\gamma}} H^o. \quad (2)$$

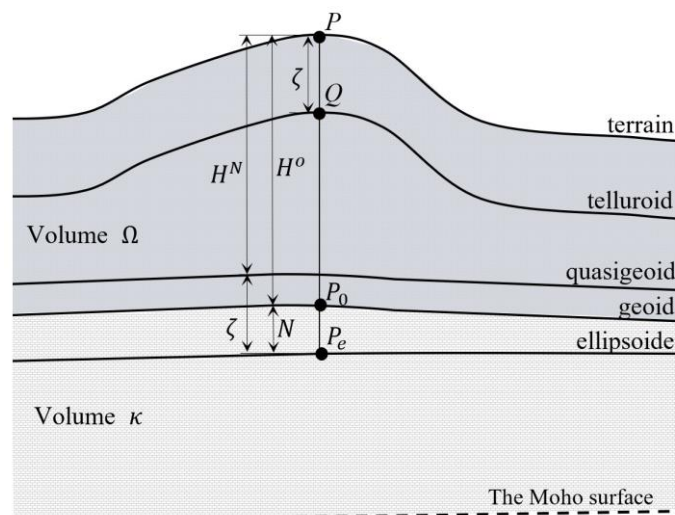


Figure 1. Schematic illustrating the quantities H^N , H^o , ζ , and N , as well as the locations of Volumes Ω and κ . Differences between the real and normal plumb lines, as well as normal to the ellipsoid, are neglected.

The Δg_B value in Equation (2) is a simple Bouguer anomaly, which is determined on the basis of the Bouguer plate reduction [1,2], and the GQS determined according to Equation (2) is also called the simple GQS.

Since the \bar{g} value is used to determine the orthometric heights, research on the exact determination of these heights also applies to the exact determination of the GQS. In this regard, many studies have been conducted in order to increase the accuracy of the \bar{g} determination and show the importance of the various factors contributing to it [3–5]. Along with the desire to determine exact orthometric heights, solutions were proposed to increase the accuracy of GQS values. An improved formula for the GQS, in relation to Equation (2), was derived by [6]. The formula includes, in addition to the effect of the simple Bouguer anomaly, a terrain correction term and a term that considers the lateral variation of the topographic density. Alternatively, ref. [7] proposed a formula for the GQS as a function of the mean value of the gravity disturbances along the plumb line within the topography. Similar to [4,5], using the decomposition of gravity, ref. [8] investigated the effect of topography on the GQS and developed a compact formulation for the rigorous treatment of topographic masses. Regarding this, ref. [9] suggested a strict formula for the GQS consisting of three components: the major term with the refined Bouguer gravity anomaly, the topographic correction, and the gravity correction. This definition of the GQS was also generalised to an arbitrary compensation model by [10]. In turn, ref. [11] presented a rigorous formula for the GQS using Taylor expansions of gravity disturbances along the vertical. The numerical and practical aspects of computing the GQS in the spatial and spectral domains were discussed by [12], and various GQS calculation methods were studied, compared, and applied in the areas of the Himalayas and Tibet by [13].

A formula analogous to that proposed by [8,9] was developed and tested by [14] in an area of Colorado, where the 1 cm geoid computation experiment was conducted. The authors estimated the individual components of the separation (the Bouguer gravity disturbance component, potential component, and gravity gradient component), as well as the contribution of the distant topographical zones to the separation.

Let us also add that the GQS, determined with additional correction terms described above that improve its accuracy, is called the complete or accurate GQS.

The main goal of the present study is to examine the possibility of determining the accurate GQS values using the method based on the geophysical gravity inversion technique (the GGI method). The approach has so far been used for the local modelling of the quasigeoid. However, the solution itself allows for the modeling of various functionals of the Earth's gravity field, including the determination of the GQS or geoid undulation.

These possibilities of the GGI method have not yet been tested. Hence, in this study, the details of the GGI solution in terms of determining the GQS and the first analyses are presented. Test calculations were conducted for an area of the Colorado mountains where the quasigeoid models were previously determined using various approaches [15], including the GGI method [16]. As mentioned above, the complete GQS values were also determined for this area using the approach proposed by [14].

2. Materials and Methods

2.1. The Utilized Solution

The GGI method was developed as a quasigeoid modeling method based on the geophysical gravity data inversion technique. Generally, it consists of building a local disturbing potential model represented by three components [17,18]:

- The potential T_{Ω} produced by the local topographic masses included in Volume Ω .
- The potential T_{κ} produced by the mass anomalies located between the geoid and the Moho surface, which are included in Volume κ . Volume κ horizontally covers the same area as Volume Ω .
- The component T_E (external disturbing potential), which represents the disturbing potential not covered by the T_{Ω} and T_{κ} components.

Volumes Ω and κ are horizontally limited, slightly beyond the study area, and do not cover all the masses producing the disturbing potential (Figure 1). Hence, the T_E component covering the influence of the masses located further away is introduced; a long wavelength nature is assumed for this component. Based on this, this component can be represented in the form of low-degree polynomials:

$$T_E = a_1 + a_2X_P + a_3Y_P + a_4X_PY_P + a_5H_P, \quad (3)$$

where a_1, \dots, a_5 are polynomial coefficients, H_P is the height of the point P , and X_P, Y_P are the coordinates of the point in the local Cartesian coordinate system. The origin of the system is located in the middle of the study area, at the geoid level. The X and Y axes lie on the horizontal plane and are directed toward the north and east, respectively. The Z axis is directed towards the geodetic zenith.

The components T_{Ω} and T_{κ} are provided by Newton's integrals:

$$T_{\Omega} = G \iiint_{\Omega} \frac{\rho}{l} dV_{\Omega}, \quad (4)$$

$$T_{\kappa} = G \iiint_{\kappa} \frac{\delta}{l} dV_{\kappa}, \quad (5)$$

where G is Newton's gravitational constant, ρ and δ are density distribution functions, dV_{Ω} and dV_{κ} are elements of volumes, and l is the distance between the computational point and the attracting masses.

Finally, the disturbing potential on the terrain surface can be defined as follows:

$$T = T_E + T_{\Omega} + T_{\kappa}. \quad (6)$$

The unknown parameters of the model (Equation (6)) are the 3D density-distribution functions ρ and δ , which are defined in Volumes Ω and κ , respectively, and the polynomial coefficients a_1, \dots, a_5 . The model parameters are determined using the least squares method based on the gravity anomalies or gravity disturbances provided in a dense network of gravity points and the disturbing potential values provided in a sparse network of points with known GNSS/levelling height anomalies, which are converted into disturbing potential values using the Bruns formula [1].

The density-distribution functions ρ and δ are determined using the procedure for the linear inversion of gravity data [19] in its discrete form. Therefore, Volumes Ω and κ were divided into finite volume blocks of constant density values. Until now, a very

simple division into constant density blocks was used in these calculations; this method assumed only one layer of lateral density variation for Volume Ω and one layer of lateral density variation for Volume κ . In applications, Volume Ω is defined by digital elevation model (DEM) blocks, which are grouped into zones of constant density (see [18], Figure 2). The constant density blocks defining Volume κ in the horizontal plane correspond to the constant density zones of Volume Ω and extend from the geoid to the Moho surface. Both Volumes Ω and κ are represented by rectangular prisms. Equations (4) and (5) can now be written in the following form [20]:

$$T_{\Omega} = \sum_{k=1}^n \left(\rho_k G \sum_{i=1}^{m_k} K_i \right), \quad (7)$$

$$T_{\kappa} = \sum_{j=1}^s (\delta_j G K_j), \quad (8)$$

where ρ_k is the determined constant density of Zone k , n is the number of zones, m_k is the number of rectangular prisms of the DEM in Zone k , δ_j is the determined density of the rectangular prism j defining the volume κ , and s is the number of prisms.

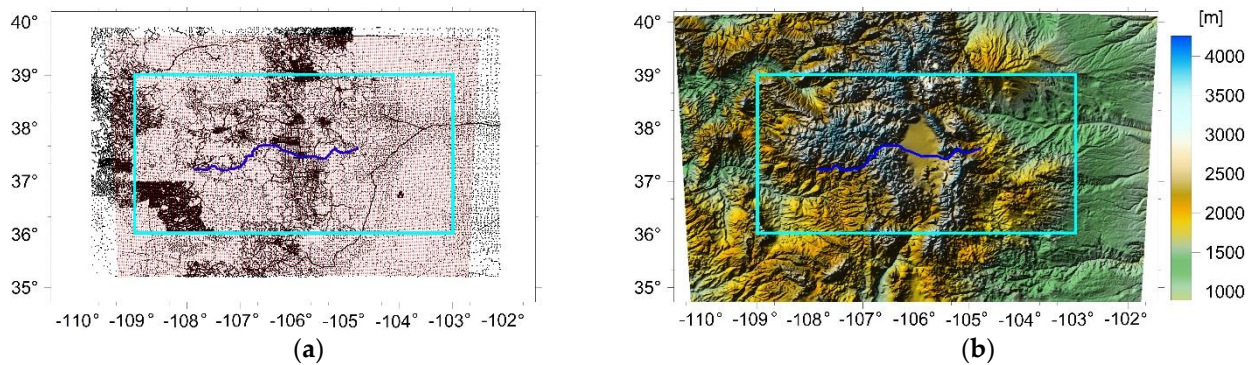


Figure 2. Data used in the calculations: (a) Terrestrial gravity points (black dots) and points of the predicted gravity-disturbance grid (red dots); (b) Relief map of the considered area. The borders of the presented DEM define the horizontal range of Volumes Ω and κ . Light-blue rectangles define the area with height anomalies obtained from the adopted quasigeoid model. The dark-blue line shows the location of the GSVS17 profile points.

The coefficients K_i and K_j are Newton's integrals for the rectangular prisms i of the DEM and j of the volume κ , respectively:

$$K_i = \int_{z_{i1}}^{z_{i2}} \int_{y_{i1}}^{y_{i2}} \int_{x_{i1}}^{x_{i2}} \frac{1}{l_i} dx_i dy_i dz_i, \quad (9)$$

$$K_j = \int_{z_{j1}}^{z_{j2}} \int_{y_{j1}}^{y_{j2}} \int_{x_{j1}}^{x_{j2}} \frac{1}{l_j} dx_j dy_j dz_j, \quad (10)$$

where x_{i1} , x_{i2} , y_{i1} , y_{i2} , z_{i1} , z_{i2} and x_{j1} , x_{j2} , y_{j1} , y_{j2} , z_{j1} , z_{j2} are the coordinates defining the rectangular prism i and j respectively; $l_i = \sqrt{(X_P - x_i)^2 + (Y_P - y_i)^2 + (Z_P - z_i)^2}$; $l_j = \sqrt{(X_P - x_j)^2 + (Y_P - y_j)^2 + (Z_P - z_j)^2}$; and $Z_P = H_P$.

The integrals in Equations (9) and (10), and their derivatives, are then replaced with exact solutions for prism ([21], Equations (4) and (8)).

In the calculations, the sphericity of the Earth is also considered. The height coordinates of the DEM blocks and the prisms of Volume κ are changed by the correction $\Delta z = -\left(R - \sqrt{R^2 - d^2}\right)$, where R is the mean Earth radius and d is the horizontal distance between the point P and the particular prism centre [16].

An important step of the calculations is the adoption of the initial density models ρ_0 for Volume Ω and δ_0 for Volume κ . The model ρ_0 is usually assumed to be constant for all topography. The model δ_0 is defined as a kind of topographic-isostatic model, whereby the masses of Volume κ balance the masses of Volume Ω . According to this, in the discrete form of the δ_0 model, the constant density value of Block j of Volume κ located exactly below the constant density zone i of Volume Ω is defined by the following equation:

$$\delta_j^0 = -\frac{H_i \rho_0}{h_j}, \quad (11)$$

where h_j is the height of Block j of Volume κ and H_i is the mean height of Zone i of Volume Ω .

The discrete initial density model defined above can be written in the following form:

$$\boldsymbol{\tau}_0^T = [\boldsymbol{\rho}_0^T, \boldsymbol{\delta}_0^T] = [\rho_1^0, \dots, \rho_n^0, \delta_1^0, \dots, \delta_s^0]. \quad (12)$$

The final density model can be written as follows:

$$\boldsymbol{\tau}^T = [\boldsymbol{\rho}^T, \boldsymbol{\delta}^T] = [\rho_1, \dots, \rho_n, \delta_1, \dots, \delta_s]. \quad (13)$$

Now, we can define the vector of unknown parameters of the model (Equation (6)) in the following form:

$$\mathbf{dx}^T = [\mathbf{a}^T, \mathbf{d}\boldsymbol{\tau}^T], \quad (14)$$

where $\mathbf{d}\boldsymbol{\tau} = \boldsymbol{\tau} - \boldsymbol{\tau}_0$ is the vector of residual densities and $\mathbf{a} = [a_1, \dots, a_5]^T$.

Considering the defined vector of unknowns (Equation (14)), the observation equation for the disturbing potential T can be written as follows [16]:

$$T + v_T = \mathbf{f}^T \mathbf{dx} + T_0, \quad (15)$$

where \mathbf{f} is the vector of known coefficients resulting from the equation of the disturbing potential model (Equation (6)), with its components defined by Equations (3)–(5).

For the gravity disturbance (δg), the appropriate equation will have the following form:

$$\delta g + v_{\delta g} = -\mathbf{f}_z^T \mathbf{dx} + \delta g_0, \quad (16)$$

where \mathbf{f}_z is the known vector resulting from taking the Z_p derivative of Equation (6).

The values v_T and $v_{\delta g}$ in Equations (15) and (16) are adjustment errors, and the approximate observation quantities are defined as:

$$T_0 = \mathbf{f}^T \mathbf{dx}_0 \quad (17)$$

and

$$\delta g_0 = -\mathbf{f}_z^T \mathbf{dx}_0 \quad (18)$$

are determined based on the vector $\mathbf{dx}_0^T = [\mathbf{a}_0^T, \boldsymbol{\tau}_0^T]$, where \mathbf{a}_0 is a five-dimensional zero vector.

Equations (15) and (16) for the series of observations form a system of equations, which we will write as follows:

$$\mathbf{v} = \mathbf{A} \mathbf{dx} - \mathbf{L}, \quad (19)$$

where \mathbf{A} is the design matrix of known coefficients, $\mathbf{L}^T = [T - T_0, \dots, \delta g - \delta g_0, \dots]$ is the vector of observations, and $\mathbf{v}^T = [v_T, \dots, v_{\delta g}, \dots]$ is the vector of adjustment errors.

To eliminate the ambiguity of the gravity data inversion, the approach suggested by [22] was used. An additional condition is imposed on the determined parameters:

$$\mathbf{dx}^T \mathbf{W}_x \mathbf{dx} = \min, \quad (20)$$

where $\mathbf{W}_x = \begin{bmatrix} \mathbf{W}_a & \mathbf{0} \\ \mathbf{0} & \mathbf{W}_\tau \end{bmatrix}$, \mathbf{W}_a is the zero weighting matrix assigned to the vector \mathbf{a} , and \mathbf{W}_τ is the density model weighting matrix. A detailed description of the definition and determination of the model-weighting matrix can be found in [18].

With the defined weight-observation matrix \mathbf{P} and considering Equation (20), the least squares objective function can be written as follows:

$$\mathbf{v}^T \mathbf{P} \mathbf{v} + \mathbf{d} \mathbf{x}^T \mathbf{W}_x \mathbf{d} \mathbf{x} = \min. \quad (21)$$

The condition defined in Equation (21) leads to the solution of the system of equations defined in Equation (19):

$$\mathbf{d} \mathbf{x} = \left(\mathbf{A}^T \mathbf{P} \mathbf{A} + \mathbf{W}_x \right)^{-1} \mathbf{A}^T \mathbf{P} \mathbf{L}. \quad (22)$$

The determined parameters of the model (the densities ρ_k and δ_j of Volumes Ω and κ , respectively, as well as the coefficients a_1, \dots, a_5) allow for the calculation of various functionals of the disturbing potential at any point in the considered area based on Equation (6). In order to determine the quasigeoid model, on the basis of the DEM, the heights of the regular grid nodes are determined; the disturbing potential values are calculated from the GGI model. These values are converted using the Bruns formula to the height anomalies (Figure 1):

$$\zeta = \frac{T(P)}{\gamma_Q} = \frac{T_E(P) + T_\Omega(P) + T_\kappa(P)}{\gamma_Q}, \quad (23)$$

where $T(P)$ is the disturbing potential calculated at Point P on the terrain surface and γ_Q is the normal gravity at the telluroid.

Let us also add that calculations can be performed with the use of global geopotential models (GGMs). In this case, the remove–compute–restore procedure is used (e.g., [16]), and the quasigeoid models determined are slightly more accurate than models built without the use of GGMs ([23,24]).

The quasigeoid model determined according to the procedure presented above (with or without the use of GGM) is fitted to GNSS/leveling height anomalies. In [16], a modification of the GGI solution was proposed that allows for the determination of gravimetric quasigeoid models, which are fitted to the particular GGM being used. In this case, the GGI model is developed without GNSS/levelling data (only GGM and gravity data are used). Both quasigeoid modeling solutions using the GGI method (fitted to GNSS/levelling data and the gravimetric solution) mentioned were used to build the current quasigeoid model for Poland ([25]).

Thus far, the disturbing potential values have been determined by the GGI approach at points on the terrain surface, allowing for the determination of the height anomalies (Equation (23)). However, the disturbing potential can be determined from the model (Equation (6)) at any point, including inside Volumes Ω and κ or at points on the geoid (Figure 1). By determining the disturbing potential at Point P_0 on the geoid ($T(P_0)$), the geoid undulation can also be determined based on the Bruns formula:

$$N = \frac{T(P_0)}{\gamma_e} = \frac{T_E(P_0) + T_\Omega(P_0) + T_\kappa(P_0)}{\gamma_e}, \quad (24)$$

where γ_e is the value of the normal gravity at Point P_e on the ellipsoid.

Hence, we can determine the GQS value directly as a difference:

$$N - \zeta = GQS = \frac{T(P_0)}{\gamma_e} - \frac{T(P)}{\gamma_Q} = GQS_{T_E} + GQS_{T_\Omega} + GQS_{T_\kappa} \quad (25)$$

where

$$GQS_{T_E} = \left(\frac{T_E(P_0)}{\gamma_e} - \frac{T_E(P)}{\gamma_Q} \right); \quad GQS_{T_\Omega} = \left(\frac{T_\Omega(P_0)}{\gamma_e} - \frac{T_\Omega(P)}{\gamma_Q} \right) \quad \text{and} \quad GQS_{T_\kappa} = \left(\frac{T_\kappa(P_0)}{\gamma_e} - \frac{T_\kappa(P)}{\gamma_Q} \right).$$

In Equations (23)–(25), the values $T(P_0)$ and $T(P)$ are determined using the same GGI model provided by Equation (6), and the parameters are estimated according to the standard GGI modeling procedure described above.

Note also that Equations (23)–(25) represent the basic form of the GGI model i.e., without a GGM. In this form of the model, the two main components of the GQS values defined in Equation (25) correspond to the main components of the complete GQS values defined by the classical approaches (e.g., [14] Equation (3)). The GQS_{T_κ} component depends on the density distribution of the masses lying below the geoid, which corresponds to the Bouguer gravity anomaly component in the classical approach, whereas the GQS_{T_Ω} component is defined almost the same as the topographic potential correction in the classical approach. Because of these similarities, we will consider and analyse this basic form of the GGI model in the following.

The points with known GNSS/levelling height anomalies necessary for the GQS values modelling can be replaced by a regular grid of height anomalies obtained from an existing quasigeoid model. This approach is recommended because GNSS/levelling points are usually arranged in an irregular grid, often with low resolution. The use of the existing quasigeoid model allows for the optimal selection of these points. This does not present any problem when we note that modeling of the GQS values with the GGI method is an extension of the functionality of this method and can be considered as a complementary step in quasigeoid modeling. In this case, much of the preparatory and computational work completed at the quasigeoid modeling can be used directly in the GQS and geoid determination. Of course, if a quasigeoid model has already been developed (using any approach) in the area being considered, the solution can only be used to implement the GQS value determination.

If the constant density of the topographic masses is assumed, or if a known model of these densities is used and will be not corrected in the GGI modelling process, the following equality will hold true: $\rho_0 = \rho$. The determined density model will, therefore, only include the densities of Volume κ and will take the following form:

$$\boldsymbol{\tau}_\delta^T = [\boldsymbol{\delta}^T] = [\delta_1, \dots, \delta_s]. \quad (26)$$

Hence, the vector of the determined model parameters (Equation (6)) will be written in the following form:

$$\mathbf{d}\mathbf{x}_\delta^T = [\mathbf{a}^T, \mathbf{d}\boldsymbol{\tau}_\delta^T], \quad (27)$$

where $\mathbf{d}\boldsymbol{\tau}_\delta = \boldsymbol{\delta} - \boldsymbol{\delta}_0$.

In this case, constant density zones of volume Ω are defined only to estimate the initial density model δ_0 (Equation (11)).

2.2. The Used Data

The analyses were conducted in the Colorado geoid computation experiment area [15]. This area is a highly mountainous area, with an average height of over 2200 m; the highest point is more than 4000 m. The basic dataset used in the calculations was provided by the US National Geodetic Survey and consists of the terrestrial gravity data and DEM. To define Volume κ , the CRUST1.0 Moho depth model ([26]) was used. In detail, we used the following datasets:

- Terrestrial gravity data (54,859 points used);
- Two DEMs with resolutions of 100 m and 500 m determined based on the SRTM v4.1 digital elevation model at a grid spacing of 3'' ([27]);
- Geoid slope validation survey (GSVS17) dataset (locations of 223 points);
- The Moho depth model with a resolution of 1°.
- The utilised datasets are presented in Figure 2.

In Figure 2, the light-blue rectangles mark the test area in which the $1' \times 1'$ grid of points was defined. The grid covers the area between the parallels 36° and 39° north

(latitude) and the meridians 103° and 109° west (longitude) and consists of 65,341 points. These points will be also referred to as the “test points” hereinafter. For this area, as part of the 1 cm Colorado geoid computation experiment, 14 quasigeoid models were built using various methods. Based on this group of models, the mean quasigeoid model was determined (ζ^{mean}); it was considered to best reflect the quasigeoid in this area ([15]). The ζ^{mean} model will be used in one part of the analyses. The other analysis will use the quasigeoid model developed using the GGI method described above ([16]). This model will be denoted as ζ_{Ref} . To verify the computed GQS values, our results were compared with the reference values, which consisted of the GQS values determined by [14]. These values were determined as the sum of three components: the Bouguer gravity-disturbance component (the main term), the topographic potential correction, and the gravity-gradient correction. These values will be denoted as GQS_{Ref} .

The dark-blue lines in Figure 2 mark the locations of the GSVS17 profile points. However, the measured GPS/leveling data at these profile points were not directly used in the present calculations. Both the geoid and quasigeoid values in this profile are the subject of numerous published analyses, and so, for comparison purposes, we have also shown the GQS values determined in this study along this profile.

3. Results

The analyses conducted primarily involved an evaluation of the described approach for determining the GQS values. As the calculations use height anomalies in addition to gravity data (which are the basic data used for the modelling procedure), the analyses will also consider these data. The modeling results also depend, to some extent, on the assumed sizes of the constant density zones. For quasigeoid modeling with the GGI approach, this parameter was analysed by [18]. Here, we will also analyse this parameter in terms of determining the GQS value. Thus, the rest of this section will present analyses regarding the following:

- The determination and evaluation of the GQS;
- The estimation of the impact of the height anomalies used on the determined GQS values;
- The estimation of the impact of the size of the constant density zones on the determined GQS values.

As different gravity data collections will be used in the first analyses, the quasigeoid heights determined from the GGI model according to Equation (23) and the GQS values according to Equation (25) will be identified using lower indices denoting the set of gravity data used.

3.1. Determination and Evaluation of the Geoid–Quasigeoid Separation

For the analyses carried out in this section, constant density zones with dimensions of 6×6 km were adopted. The calculations used height anomalies determined at 65,341 test points based on the ζ_{Ref} model. From this set, 1891 points were selected to form a regular grid with a resolution of approximately 11×9 km. This set of known height anomalies and the previously described terrestrial gravity data were used to develop the GGI model. Considering the terrestrial gravity data used, the height anomalies and GQS values determined by Equations (23) and (25) will be denoted as ζ_T and GQS_T , respectively.

In order to analyse the influence of the utilised density of topographic masses on the parameters determined, three versions of the model were developed with the following initial densities ρ_0 : 2200 kg/m³, 2400 kg/m³, and 2670 kg/m³. For each version, the values of ζ_T and GQS_T were determined for the test points, and for each version, the differences were calculated:

$$\Delta\zeta_T = \zeta_T - \zeta_{Ref}. \quad (28)$$

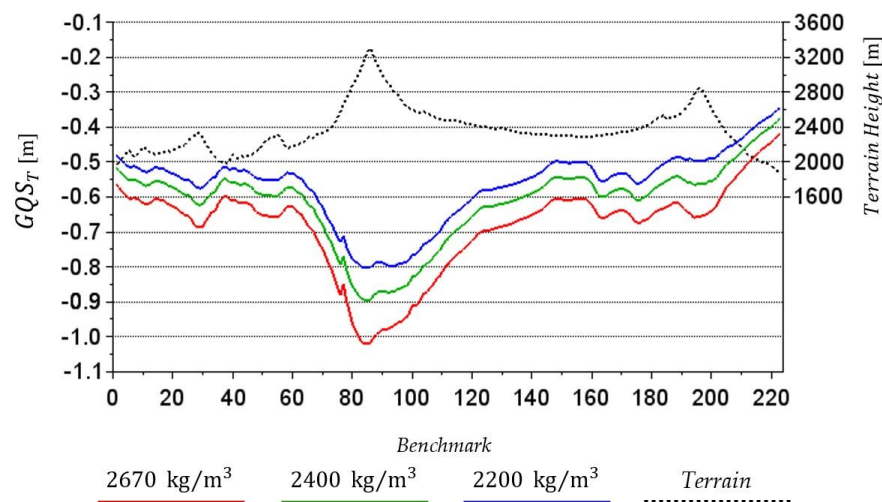
The basic statistics of both the GQS_T and $\Delta\zeta_T$ values for individual model versions with different values of ρ_0 are presented in Table 1.

Table 1. Basic statistics of GQS_T and $\Delta\zeta_T$ values determined for test points for various model versions with different values of the density ρ_0 .

	ρ_0	Min.	Max.	Mean	Std. Dev.
Unit	[kg/m ³]	[m]	[m]	[m]	[m]
GQS_T	2200	−0.995	−0.136	−0.434	0.173
	2400	−1.112	−0.149	−0.478	0.195
	2670	−1.296	−0.168	−0.538	0.225
$\Delta\zeta_T$	2200	−0.105	0.078	0.000	0.007
	2400	−0.108	0.076	0.000	0.007
	2670	−0.111	0.081	0.000	0.009

The results presented in Table 1 clearly show that the changes in the density of topographic masses actually have little influence on the height anomalies determined from the GGI model. The individual statistics of the $\Delta\zeta_T$ values for all versions are very similar or the same. This is not the case for the GQS values, which differ significantly between different versions of the model. The absolute values of all statistics increase with increasing density, and the increase rate is almost constant. The mean GQS value changes by about 0.022 m for every 100 kg/m³ of change in the density, and the difference between the minimum values for the extreme analysed densities reaches 0.30 m.

The GQS_T values for the three analysed versions for the GSVS17 profile points are presented in Figure 3. It is clear that the general course of the GQS values reflects the terrain heights. However, the lines for the different model versions are nearly parallel, although the distances between them clearly increase with the terrain height.

**Figure 3.** The GQS_T values for the three versions of the model with different density values of the topographic masses and terrain heights at the GSVS17 profile points.

We should also add that, considering the good agreement between the ζ_T and ζ_{Ref} values for the different versions of the model, the geoid undulations will differ to a similar extent as the GQS values. Thus, the presented analyses indicate that both the geoid undulations and the GQS values determined from the GGI model significantly depend on the adopted, initial topographic mass densities.

The most important part of this research is the verification of the determined GQS values. As mentioned previously, our results were compared with the GQS_{Ref} values. Since the GQS_{Ref} values were determined by assuming a constant density of topographic masses equal to 2670 kg/m³ ([14]), for comparison purposes, all further calculations and analyses will be performed assuming that $\rho_0 = 2670$ kg/m³. Therefore, the version of the

GGI model determined for this value of the initial density was used, and the differences were calculated as follows:

$$\Delta GQS_T = GQS_T - GQS_{Ref}. \quad (29)$$

The most important statistics of the quantities defined by Equation (29) are presented in the first row of Table 2.

Table 2. Basic statistics of the differences ΔGQS_T , ΔGQS_G , and ΔGQS_{TG} (unit: m).

	Min.	Max.	Mean	Std. Dev.
ΔGQS_T^*	−0.132	0.075	−0.002	0.010
ΔGQS_G^*	−0.056	0.060	−0.001	0.007
ΔGQS_{TG}^*	−0.059	0.075	−0.001	0.007
ΔGQS_{TG}^{**}	−0.016	0.021	−0.002	0.006

* Determined for test points; ** Determined for GSV517 profile points.

When analysing the presented statistics for ΔGQS_T , it should be noted that the determined and reference GQS values are compatible. The average value of the ΔGQS_T differences is -0.002 m, and their standard deviation is 0.010 m, although the greatest difference reaches -0.132 m. Figure 4a shows the spatial distribution of the ΔGQS_T differences.

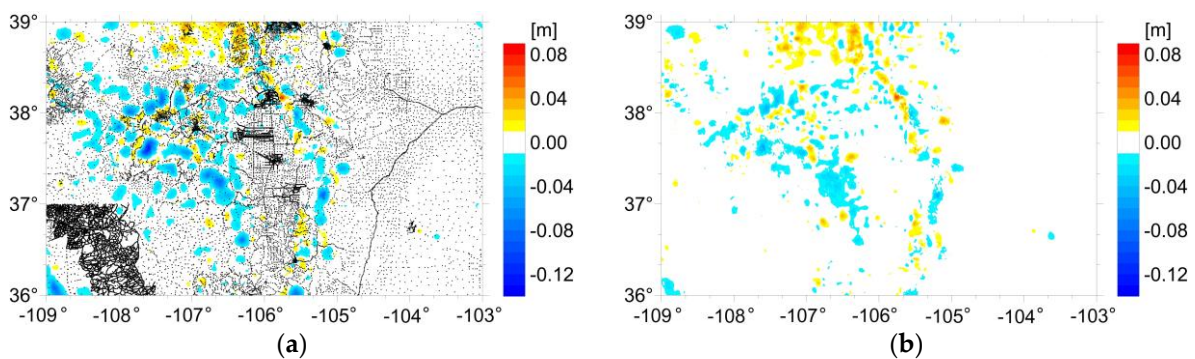


Figure 4. The differences between the determined and reference GQS values: (a) the ΔGQS_T values; (b) the ΔGQS_{TG} values. The small black dots in Panel (a) represent terrestrial gravity points.

The black dots in Figure 4a mark the location of terrestrial gravity points. It can be seen that the ΔGQS_T differences are very small in most of the study area. Greater differences are visible in the areas with the highest mountains, and they are largest in the areas where there are no gravity data. Larger ΔGQS_T values in areas not covered by the gravity data were expected and result from the different interpolation properties of both compared approaches. Hence, in the next step, for areas not covered by the gravity data, the gravity disturbances (which are used in the GGI approach) were predicted. The prediction process was conducted in three stages:

1. The determination of the Bouguer gravity disturbances (δg_B) for all gravity points by removing the topographic reduction (δg_{Top}) [2], known also as refined Bouguer reduction:

$$\delta g_B = \delta g - \delta g_{Top}. \quad (30)$$

2. The construction of a regular grid (48,439 nodes) of Bouguer disturbances with a resolution of 2×2 km using the kriging method (we used the “Surfer 24” software for this purpose).

3. The determination of the gravity disturbances at the grid points, restoring the topography reduction.

The points of the determined grid are marked in Figure 1 with red dots. From this grid, a group of 22,155 nodes were selected for which there was no terrestrial gravity

point within 2 km. This group of points formed a complementary gravity dataset for the terrestrial gravity data. With the use of the predicted data, two further GQS models were built. One, using all the points of the predicted grid (without the previously used terrestrial gravity data), was denoted as GQS_G and the other, based on a set of terrestrial gravity points supplemented by the abovementioned complementary gravity dataset, was denoted as GQS_{TG} . Both models also used the same points with known height anomalies that were used previously. The statistics of these values are presented in the Table 3.

Table 3. Basic statistics of the GQS_G and GQS_{TG} values, determined for test points (unit: m).

	Min.	Max.	Mean	Std. Dev.
GQS_G	−1.259	0.168	−0.536	0.223
GQS_{TG}	−1.273	−0.168	−0.537	0.224

The modelling results were again compared with the reference GQS model by determining the differences as follows:

$$\Delta GQS_G = GQS_G - GQS_{Ref}, \quad (31)$$

$$\Delta GQS_{TG} = GQS_{TG} - GQS_{Ref}. \quad (32)$$

The basic statistics of these differences are presented in Table 2.

To briefly summarise this part of the research, it should be noted that the use of the predicted gravity disturbances in areas where gravity data are missing positively affects the modelling results. The largest values of both ΔGQS_G and ΔGQS_{TG} decreased by over 50% in relation to ΔGQS_T . The standard deviations are also smaller (0.007 m). Therefore, when using the GGI method to estimate the GQS values, it is worth supplementing the gaps in gravity data with predicted values, or using only a regular grid of predicted values. The selection of the best prediction method is a separate issue. Note also that the reported statistics of the ΔGQS_G and ΔGQS_{TG} values are at a similar level. Therefore, the applications of both analysed approaches to the distribution of gravity data can be considered equivalent.

Considering this, further analyses were based on a set of terrestrial gravity points supplemented by the complementary gravity datagrid.

The spatial distribution of the ΔGQS_{TG} values is presented in Figure 4b.

The ΔGQS_{TG} differences were also determined for the GSVS17 profile points. These differences are presented in Figure 5, and their most important statistics are provided in the last row of Table 2. The agreement of the GQS_{TG} model with the GQS_{Ref} model is slightly better for profile points than for the entire area, and larger differences between the models are visible at the highest mountain parts of the profile.

The map of the GQS_{TG} is presented in Figure 6.

The GQS model determined on the basis of Equation (25) can be split into the individual components: GQS_{T_Ω} , GQS_{T_k} , and GQS_{T_E} . Table 4 presents the basic statistics of the components that constitute the GQS_{TG} model.

Table 4. Basic statistics of the components of the GQS_{TG} model (unit: m).

	Min.	Max.	Mean	Std. Dev.
GQS_{T_Ω}	−0.230	0.182	−0.046	0.026
GQS_{T_k}	−1.353	−0.157	−0.509	0.219
GQS_{T_E}	0.009	0.033	0.018	0.005

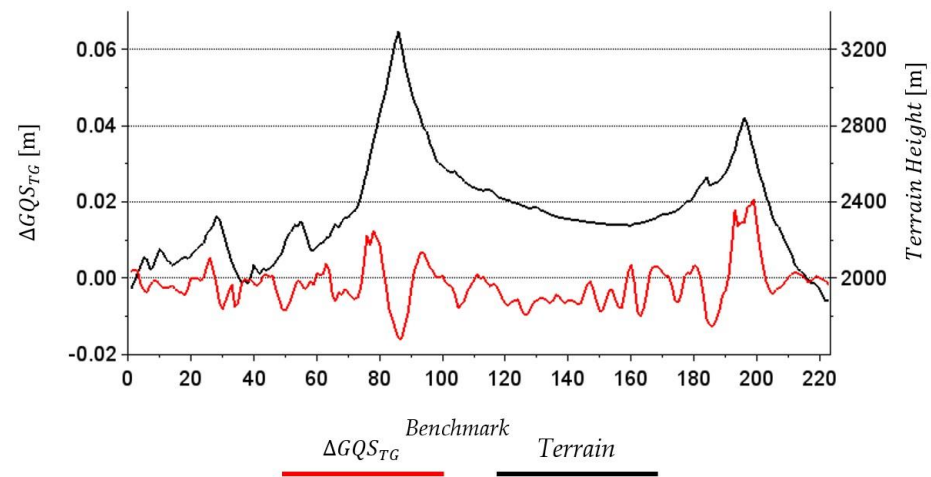


Figure 5. The ΔGQS_{TG} values and terrain heights at the GSVS17 profile points.

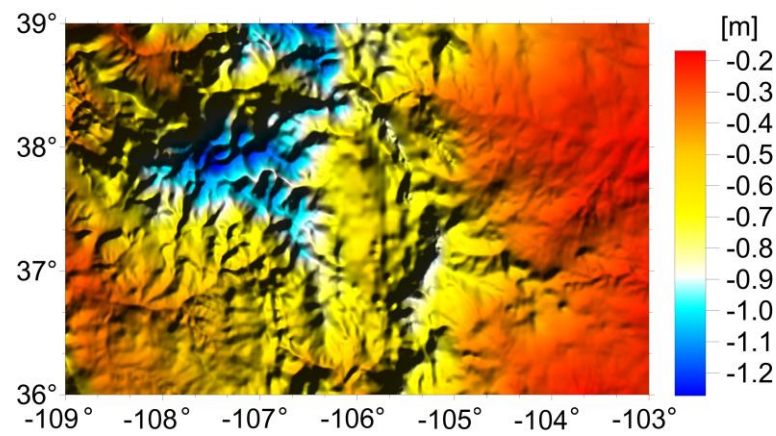


Figure 6. The GQS_{TG} values.

Maps of the components $GQS_{T\Omega}$, $GQS_{T\kappa}$, and $GQS_{T\epsilon}$ of the GQS_{TG} are presented in Figures 7–9, respectively.

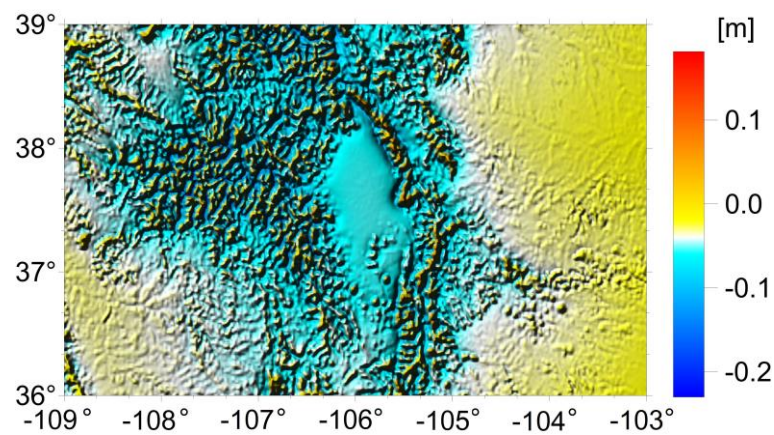


Figure 7. The values of the GQS_{Tn} component of the GQS_{TG} model.

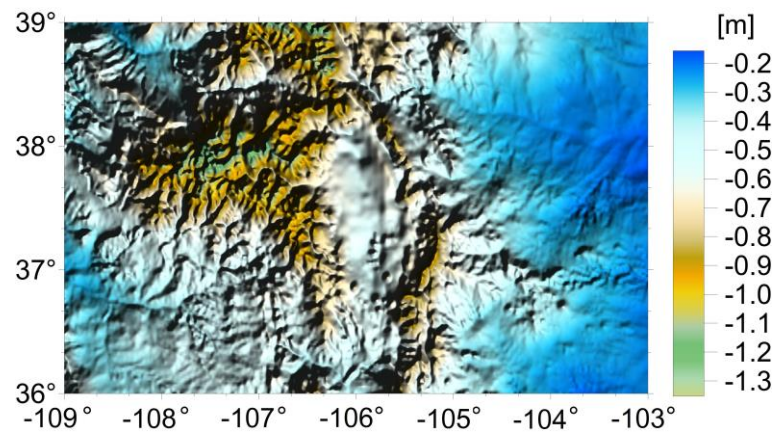


Figure 8. The values of the GQS_{T_x} component of the GQS_{T_G} model.

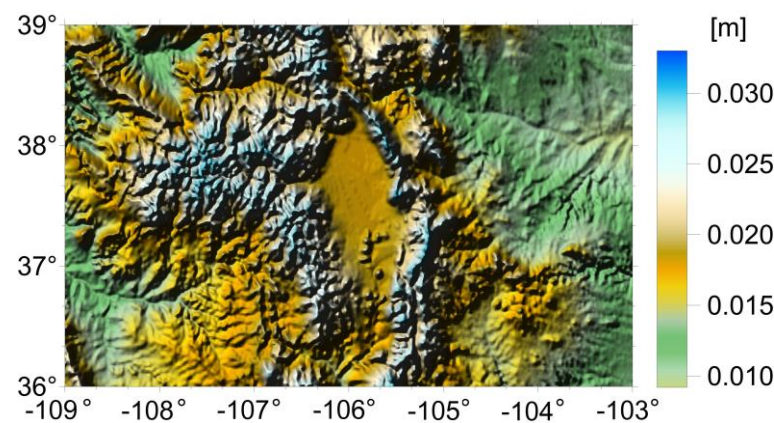


Figure 9. The values of the GQS_{T_E} component of the GQS_{T_G} model.

The presented results clearly indicate that the component GQS_{T_x} (Figure 8), which is associated with the density distribution in the zone below the geoid, has the greatest impact on the values of the determined GQS (Figure 6). This also corresponds to the other methods ([14,28,29]) in which the dominant component is determined based on the Bouguer gravity anomaly, which also mainly depends on the density distribution of the masses lying below the geoid. Figure 7 presents the values of the component related to the topography (GQS_{T_Q}), which are much smaller but also significant, varying between -0.230 m and 0.182 m. The component GQS_{T_E} has the least importance for the determined GQS values. Although it only changes in the range from 0.009 – 0.033 m, it reflects the topography very accurately (compare Figure 9 with Figure 2b). This is due to the way the T_E component is calculated (Equation (3)); only the last part ($a_5 H_p$) depends on the heights of the points, affecting the variation of the GQS values, while the other parts have no effect on the GQS values.

3.2. Estimation of the Impact of Height Anomalies Used in the Calculations on the Determined GQS Values

Gravity data are the basis of the GQS values determined using the analysed approach. However, the GGI model also depends on the height anomalies used. To analyse the impact of these data on the modeling results, two supplementary tests were performed. They consisted of examining the influence of two factors on the determined GQS values:

- The use of different resolutions of the height anomaly grid;
- The use of another quasigeoid model in the modelling process.

Both tests used the same gravity dataset that was utilized in the previous section (terrestrial gravity points supplemented by the complementary gravity grid).

Let us recall that the research described in Section 3.1 used height anomalies on a regular grid with a resolution of approximately 11×9 km. The test concerning the impact of different resolutions of the height anomaly grid on GQS values used two additional grids of points with known height anomalies with resolutions of approximately 5.5×4.5 km and 22×18 km. Both grids are based on the same quasigeoid model used previously. Thus, within this test, three GQS sets obtained from different height anomaly grids (11×9 km, 5.5×4.5 km, 22×18 km) were investigated.

First, we compared the determined GQS and height anomalies of each version to their reference values (GQS_{Ref} and ζ_{Ref} values respectively). The basic statistics of the differences for each version are included in Table 5.

Table 5. Statistics of the differences between different versions of the GQS and height anomalies for various grid resolutions of the known height anomalies and their reference values GQS_{Ref} and ζ_{Ref} , respectively. Quantities were determined for test points. The data in the second row were taken from Table 2.

	Grid Resolution	Min.	Max.	Mean	Std. Dev.
Unit	[km]	[m]	[m]	[m]	[m]
$GQS_{TG} - GQS_{Ref}$	5.5×4.5	−0.072	0.072	−0.002	0.008
	11×9	−0.059	0.075	−0.001	0.007
	22×18	−0.062	0.076	−0.001	0.007
$\zeta_{TG} - \zeta_{Ref}$	5.5×4.5	−0.090	0.066	0.000	0.008
	11×9	−0.130	0.080	0.000	0.013
	22×18	−0.161	0.087	0.000	0.022

Individual versions of GQS were also compared with each other. The basic statistics of the differences between the versions are presented in Table 6.

Table 6. Statistics of the differences between GQS values for each version of the height anomaly grid determined for test points. The upper superscript indicates the resolution of height anomaly grid used (unit: m).

	Min.	Max.	Mean	Std. Dev.
$GQS_{TG}^{11 \times 9} - GQS_{TG}^{22 \times 18}$	−0.023	0.007	0.000	0.002
$GQS_{TG}^{11 \times 9} - GQS_{TG}^{5.5 \times 4.5}$	−0.016	0.038	0.000	0.002
$GQS_{TG}^{22 \times 18} - GQS_{TG}^{5.5 \times 4.5}$	−0.017	0.045	0.001	0.004

The results presented in Tables 5 and 6 indicate that the resolution of the adopted grid of height anomalies has an impact on both analysed quantities (the GQS and height anomalies). This impact is clearly smaller in the case of the GQS values. Although the differences between particular versions of the model with different height anomaly grids provided in Table 6 reach 0.045 m, their standard deviations are in the range of 0.002–0.004 m. The differences between GQS versions are also not clearly visible in the statistics related to reference values presented in Table 5. These statistics are almost the same, although slightly better results can be observed for the lower-resolution versions.

This is not the case when it comes to the fit of the analysed versions of height anomalies to the reference quasigeoid model. As the grid resolution of the height anomalies used decreases, most of the analysed statistics (except for the mean value) increase (Table 5), which means that the accuracy of the quasigeoid model decreases. Larger changes in the height anomalies and smaller changes in the GQS values indicate that the N and ζ values determined based on Equations (23) and (24), respectively, are partially distorted by errors of a similar nature. When determining the GQS values according to Equation

(25), such errors cancel each other out. This relationship is also noticeable in the second test described below.

The second test conducted in this section involved using another quasigeoid model in the modelling process. For this purpose, the ζ^{mean} model was used. From this model, a grid of height anomalies with a resolution of 11×9 km was selected. The locations of the points of this grid were the same as in previous analyses. The gravity dataset remained unchanged. Based on these data, the height anomalies (ζ_{TG}^{mean}) and GQS values (GQS_{TG}^{mean}) were determined according to Equations (23) and (25), respectively. These values were compared with the GQS_{Ref} and the previously determined values of ζ_{TG} and GQS_{TG} . The statistics of the differences between the compared values are presented in Table 7.

Table 7. Statistics of the differences between the GQS values and height anomalies determined for test points using different quasigeoid models (unit: m).

	Min.	Max.	Mean	Std. Dev.
$GQS_{TG}^{mean} - GQS_{Ref}$	−0.064	0.070	−0.001	0.007
$GQS_{TG} - GQS_{TG}^{mean}$	−0.012	0.020	0.000	0.002
$\zeta_{TG} - \zeta_{TG}^{mean}$	−0.035	0.103	0.014	0.019

The statistics included in Table 7 show that the adoption of different quasigeoid models for the calculations has a very small impact on the determined GQS values. The greatest difference between the GQS_{TG} and the GQS_{TG}^{mean} values is 0.020 m, and the standard deviation is only 0.002 m. The statistics of the $GQS_{TG}^{mean} - GQS_{Ref}$ differences are also very similar to the statistics of the $GQS_{TG} - GQS_{Ref}$ differences determined for the same grid of height anomalies (Table 5). However, the differences in the determined height anomalies are much larger and reach the level of 0.10 m, and their standard deviation is 0.019 m. This clearly indicates that changes in the quasigeoid model used in the calculations cause changes of a similar nature in the height anomalies and geoid undulation determined using Equations (23) and (24), respectively.

Considering that, when determining the geoid undulation model using the GGI approach, it is better to use the equation (instead of Equation (24)):

$$N = GQS + \zeta, \quad (33)$$

where ζ is the model used in the procedure for determining GQS values.

3.3. Estimation of the Impact of the Size of the Constant Density Zones on the Determined GQS Values

As mentioned in the description of the method, DEM blocks are grouped into zones of constant densities, and Volume κ is defined by constant density blocks, which in the horizontal plane correspond to the defined zones. The effect of the size of the constant density zones on the modeling results was analysed, along with the determination of the density model-weighting matrix coefficients, by [18]. It was demonstrated that smaller sizes of these zones lead to slightly better modeling results, and the highest accuracies of the determined quasigeoid models are obtained with zones smaller than ca. 100 km^2 . In the present study, we also analysed this parameter in terms of determining the GQS. However, we should remember that, in the present analyses, due to the assumption of the constant density of topographic masses, the different sizes of the constant density zones indicate only that the constant density blocks defining Volume κ have different sizes.

Considering that this research is being conducted in a high, mountainous area, we adopted the following constant density zone sizes for the analyses: 4×4 km, 6×6 km, 8×7.5 km, and 10×10 km. The calculations were performed using a previously used grid of height anomalies (with a resolution of 11×9 km) and gravity dataset (terrestrial gravity points supplemented by the complementary gravity dataset). Note that Quantities ζ_{TG} and

GQS_{TG} were determined previously for the 6×6 km constant density zones. Thus, the set of analysed model versions has been completed with the remaining three constant density zone sizes.

First, we compared the GQS and height anomalies for each version with the reference values GQS_{Ref} and ζ_{Ref} , respectively. The statistics of these differences are presented in Table 8.

Table 8. Statistics of the differences between the GQS_{TG} and ζ_{TG} values determined for various constant density zone sizes and the GQS_{Ref} and ζ_{Ref} values. Statistics determined for the test points.

	Size of a Single Block of Volume κ	Min.	Max.	Mean	Std. Dev.
Unit	[km]	[m]	[m]	[m]	[m]
$GQS_{TG} - GQS_{Ref}$	4×4	-0.060	0.058	-0.001	0.007
	6×6	-0.059	0.075	-0.001	0.007
	8×7.5	-0.057	0.061	-0.001	0.007
	10×10	-0.063	0.118	-0.001	0.008
$\zeta_{TG} - \zeta_{Ref}$	4×4	-0.129	0.082	0.000	0.013
	6×6	-0.129	0.080	0.000	0.013
	8×7.5	-0.129	0.077	0.000	0.013
	10×10	-0.127	0.092	0.000	0.014

The statistics of both analysed quantities, reported in Table 8, are almost the same for versions with constant density zone sizes smaller than 10×10 km, and only for the 10×10 km version are they slightly larger. So, with respect to the reference values, the impact of the size of constant density zones in the analysed case can be considered insignificant for constant density zones equal or smaller than about 8×8 km.

The versions of GQS and height anomalies for the smallest size of a constant density zone (4×4 km) were also compared to the three other versions. Table 9 presents the statistics of the differences between analysed values.

Table 9. Statistics of the differences between GQS values and height anomalies determined for a constant density zone size of 4×4 km and the three remaining constant density zone sizes. The upper superscript indicates the constant density zone size used. All compared values were determined for the test points (unit: m).

	Min.	Max.	Mean	Std. Dev.
$GQS_{TG}^{4 \times 4} - GQS_{TG}^{6 \times 6}$	-0.040	0.035	0.000	0.002
$GQS_{TG}^{4 \times 4} - GQS_{TG}^{8 \times 7.5}$	-0.040	0.034	0.000	0.004
$GQS_{TG}^{4 \times 4} - GQS_{TG}^{10 \times 10}$	-0.081	0.051	0.000	0.006
$\zeta_{TG}^{4 \times 4} - \zeta_{TG}^{6 \times 6}$	-0.021	0.008	0.000	0.001
$\zeta_{TG}^{4 \times 4} - \zeta_{TG}^{8 \times 7.5}$	-0.020	0.019	0.000	0.002
$\zeta_{TG}^{4 \times 4} - \zeta_{TG}^{10 \times 10}$	-0.048	0.032	0.000	0.004

The differences of the GQS values presented in Table 9 are small and reach 0.081 m for the version with a constant density zone size of 10×10 km. For the two smaller zone sizes, the extreme values of these differences are smaller (0.04 m) and virtually the same. The standard deviations of the differences are in the range of 0.002–0.006 m and increase with the increase in the size of constant density zone. The statistics of the differences relating to height anomalies are smaller. This indicates a clearly smaller impact of the analysed parameter on the determined quasigeoid model than on the GQS values.

4. Discussion

The main goal of this research was to attempt to determine the accurate GQS values using the GGI method. The differences between the GQS values determined from the GGI model and their reference values presented in Section 3.1 are small; in the analysed area, they reach 0.075 m, while the standard deviation of these differences is 0.007 m. Such results were obtained when the areas not covered by the measured gravity data were supplemented by the predicted values, and the largest differences occurred in areas with predicted data. Equally good results were obtained using only the predicted gravity data in the form of a regular grid.

The impact of the height anomalies used on the determined GQS values was also analysed. It has been shown that the impact of both analysed factors (different resolutions of the height anomaly grid and the use of different quasigeoid model in the modelling process) is noticeable. However, it is not significant for the statistics of the differences between the determined and reference GQS values estimated in Section 3.1. For the analysed cases, the standard deviations of these differences do not exceed 0.008 m, and their maximum values reach 0.076 m.

In analyses of the impact of the assumed size of constant density zones on the determined GQS values, it has been shown that for the size of constant density zone less than or equal to 8×7.5 km, the statistics of the differences between the determined and reference GQS values do not exceed the values estimated in Section 3.1 (although differences between the analysed cases are noticeable). For the largest of the analysed sizes of constant density zones (10×10 km), the maximum value of the differences reaches 0.118 m. Hence, we recommend using constant density zone sizes no larger than about 8×8 km.

A significant impact of the resolution of the height anomalies used on the geoid undulations determined based on Equation (24) was observed. Since this impact is very small on GQS values, we suggest that the determination of the geoid undulations should be based on an independent quasigeoid model and the determined GQS values (Equation (33)).

The obtained results also indicate some difficulties. The demonstrated impact of changes in the density of the topography on the determined GQS values (and, thus, on the geoid undulations) should be considered significant. The maximum differences reached 0.30 m for the extreme analysed densities.

It should be also noted that the solution presented can be regarded either as an independent approach to the GQS modeling problem or as an extension of the process of modeling the quasigeoid using the GGI method. In the latter scenario, a large part of the preparatory and computational work undertaken during the quasigeoid modeling phase can be directly repurposed for the GQS determination. Consequently, the GQS values can be determined with minimal additional effort.

Author Contributions: Conceptualization, M.T. and M.O.-W.; methodology, M.T. and M.O.-W.; software, M.T. and M.O.-W.; validation, Y.M.W. and M.O.-W.; formal analysis, M.O.-W.; investigation, M.O.-W.; resources, Y.M.W. and M.O.-W.; data curation, M.O.-W.; writing—original draft preparation, M.T. and M.O.-W.; writing—review and editing, M.T., M.O.-W. and Y.M.W.; visualization, M.O.-W.; supervision, M.T. All authors have read and agreed to the published version of the manuscript.

Funding: The APC/BPC is financed by Wrocław University of Environmental and Life Sciences.

Data Availability Statement: The quasigeoid, geoid and GQS models that were generated and analysed during the current study are available from the corresponding author on reasonable request.

Conflicts of Interest: The authors declare no conflict of interest.

References

1. Heiskanen, W.A.; Moritz, H. *Physical Geodesy*; W. H. Freeman and Company: San Francisco, CA, USA; London, UK, 1967.
2. Torge, W. *Geodesy*, 3rd ed.; Walter de Gruyter: Berlin, Germany; New York, NY, USA, 2001.
3. Hwang, C.; Hsiao, Y.S. Orthometric corrections from leveling, gravity, density and elevation data: A case study in Taiwan. *J. Geod.* **2003**, *77*, 279–291. [[CrossRef](#)]

4. Tenzer, R.; Vaníček, P.; Santos, M.; Featherstone, W.E.; Kuhn, M. The rigorous determination of orthometric heights. *J. Geod.* **2005**, *79*, 82–89. [[CrossRef](#)]
5. Santos, M.C.; Vaníček, P.; Featherstone, W.E.; Kingdon, R.; Ellmann, A.; Martin, B.-A.; Kuhn, M.; Tenzer, R. The relation between rigorous and Helmert's definitions of orthometric heights. *J. Geod.* **2006**, *80*, 691–704. [[CrossRef](#)]
6. Sjöberg, L.E. A refined conversion from normal height to orthometric height. *Stud. Geophys. Geod.* **2006**, *50*, 595–606. [[CrossRef](#)]
7. Tenzer, R.; Moore, P.; Novák, P.; Kuhn, M.; Vaníček, P. Explicit formula for the geoid-to-quasigeoid separation. *Stud. Geophys. Geod.* **2006**, *50*, 607–618. [[CrossRef](#)]
8. Flury, J.; Rummel, R. On the geoid–quasigeoid separation in mountain areas. *J. Geod.* **2009**, *83*, 829–847. [[CrossRef](#)]
9. Sjöberg, L.E. A strict formula for geoid-to-quasigeoid separation. *J. Geod.* **2010**, *84*, 699–702. [[CrossRef](#)]
10. Sjöberg, L.E. The geoid-to-quasigeoid difference using an arbitrary gravity reduction model. *Stud. Geophys. Geod.* **2012**, *56*, 929–933. [[CrossRef](#)]
11. Sjöberg, L.E. Rigorous geoid-from-quasigeoid correction using gravity disturbances. *J. Geod. Sci.* **2015**, *5*, 115–118. [[CrossRef](#)]
12. Tenzer, R.; Hirt, C.; Claessens, S.; Novák, P. Spatial and spectral representations of the geoid-to-quasigeoid correction. *Surv. Geophys.* **2015**, *36*, 627–658. [[CrossRef](#)]
13. Foroughi, I.; Tenzer, R. Comparison of different methods for estimating the geoid-to-quasi-geoid separation. *Geophys. J. Int.* **2017**, *210*, 1001–1020. [[CrossRef](#)]
14. Wang, Y.M.; Véronneau, M.; Huang, J.; Ahlgren, K.; Krcmaric, J.; Li, X.; Avalos-Naranjo, D. Accurate computation of geoid-quasigeoid separation in mountainous region—A case study in Colorado with full extension to the experimental geoid region. *J. Geod. Sci.* **2023**, *13*, 20220128. [[CrossRef](#)]
15. Wang, Y.M.; Sánchez, L.; Agren, J.; Huang, J.; Forsberg, R.; Abd-Elmotaal, H.; Barzaghi, R.; Bašić, T.; Carrion, D.; Claessens, S.; et al. Colorado geoid computation experiment—Overview and summary. *J. Geod.* **2021**, *95*, 127. [[CrossRef](#)]
16. Trojanowicz, M.; Owczarek-Wesołowska, M.; Wang, Y.M.; Jamroz, O. Quasi Geoid and Geoid Modeling with the Use of Terrestrial and Airborne Gravity Data by the GGI Method—A Case Study in the Mountainous Area of Colorado. *Remote Sens.* **2021**, *13*, 4217. [[CrossRef](#)]
17. Trojanowicz, M. Local modelling of quasigeoid heights with the use of the gravity inverse method—Case study for the area of Poland. *Acta Geodyn. Geomater.* **2012**, *9*, 5–18.
18. Trojanowicz, M. Local quasigeoid modelling using gravity data inversion technique—Analysis of fixed coefficients of density model weighting matrix. *Acta Geodyn. Geomater.* **2012**, *9*, 269–281.
19. Blakely, R.J. *Potential Theory in Gravity and Magnetic Applications*; Cambridge University Press: Cambridge, UK, 1995.
20. Trojanowicz, M.; Osada, E.; Karsznia, K. Precise local quasigeoid modelling using GNSS/levelling height anomalies and gravity data. *Surv. Rev.* **2020**, *52*, 76–83. [[CrossRef](#)]
21. Nagy, D.; Papp, G.; Benedek, J. The gravitational potential and its derivatives for the prism. *J. Geod.* **2000**, *74*, 552–560. [[CrossRef](#)]
22. Li, Y.; Oldenburg, D.W. 3-D inversion of gravity data. *Geophysics* **1998**, *63*, 109–119. [[CrossRef](#)]
23. Trojanowicz, M. Estimation of optimal quantitative parameters of selected input data used in local quasigeoid modelling by the GGI method. *J. Spat. Sci.* **2015**, *60*, 167–178. [[CrossRef](#)]
24. Trojanowicz, M. Local disturbing potential model with the use of geophysical gravity data inversion case study in the area of Poland. *Acta Geodyn. Geomater.* **2019**, *16*, 293–299. [[CrossRef](#)]
25. Trojanowicz, M.; Owczarek-Wesołowska, M. PL-geoid2021: A quasigeoid model for Poland developed using geophysical gravity data inversion technique. *Acta Geod. Geophys.* **2023**, *58*, 321–343. [[CrossRef](#)]
26. Laske, G.; Masters, G.; Ma, Z.; Pasyanos, M. Update on CRUST1.0—A 1-degree Global Model of Earth's Crust. *Geophys. Res. Abstr.* **2013**, *15*, Abstract EGU2013-2658.
27. Jarvis, A.; Reuter, H.I.; Nelson, A.; Guevara, E. Hole-Filled SRTM for the Globe Version 4. International Centre for Tropical Agriculture (CIAT). 2008. Available online: <http://srtm.csi.cgiar.org> (accessed on 21 February 2024).
28. Jiang, T.; Dang, Y.; Zhang, C. Gravimetric geoid modeling from the combination of satellite gravity model, terrestrial and airborne gravity data: A case study in the mountainous area, Colorado. *Earth Planets Space* **2020**, *72*, 189. [[CrossRef](#)]
29. Belay, E.Y.; Godah, W.; Szelachowska, M.; Tenzer, R. ETH-GQS: An estimation of geoid-to-quasigeoid separation over Ethiopia. *Geod. Geodyn.* **2022**, *13*, 31–37. [[CrossRef](#)]

Disclaimer/Publisher's Note: The statements, opinions and data contained in all publications are solely those of the individual author(s) and contributor(s) and not of MDPI and/or the editor(s). MDPI and/or the editor(s) disclaim responsibility for any injury to people or property resulting from any ideas, methods, instructions or products referred to in the content.